ARTICLE

Electrical Tuning of Surface Plasmon Polariton Propagation in Graphene–Nanowire Hybrid Structure

Haoliang Qian,[†,#] Yaoguang Ma,[§,#] Qing Yang,[†,#,*] Bigeng Chen,[†] Ying Liu,[‡] Xin Guo,[†] Shisheng Lin,[⊥] Jili Ruan,[†] Xu Liu,[†] Limin Tong,[†] and Zhong Lin Wang[‡,∥,*]

[†]State Key Laboratory of Modern Optical Instrumentation, Department of Optical Engineering, Zhejiang University, Hangzhou 310027, People's Republic of China, [‡]School of Material Science and Engineering, Georgia Institute of Technology, Atlanta, Georgia 30332-0245, United States, [§]State Key Laboratory for Mesoscopic Physics and Department of Physics, Peking University, Beijing 100871, People's Republic of China, [⊥]Department of Information Science and Electronic Engineering, Zhejiang University, Hangzhou 310027, People's Republic of China, and [∥]Satellite Research Facility, MANA, International Center for Materials Nanoarchitectonics, National Institute for Materials Science, 1-1 Namiki, Tsukuba, 305-0044, Japan. [#]H. Qian, Y. Ma, and Q. Yang contributed equally to this work.

ABSTRACT We demonstrate a dynamic surface plasmonic modulation based on graphene–nanowire (grapheme–NW) hybrid structures in the visible light range. A static modulation depth of as high as 0.07 dB/μm has been achieved experimentally. Through careful simulation and systematical experimental investigation, we found that the dual-confinement effect of charge density and electromagnetic energy around the vicinity of the NW will dramatically enhance the light–matter interaction and increase the Fermi level shifting, which are the key roles for bringing the optical response of the device to the visible range. The carrier concentration near the vicinity of a Ag NW is estimated to reach 0.921×10^{14} cm^{-2} after applying more than 25 V voltages, which is enough to shift the Fermi level for visible light. Furthermore, the modulation behaviors near the Dirac point of monolayer graphene and the singularity of gap-induced bilayer graphene are investigated. Calculated optical conductivity as a function of Fermi level predicts a minimum value near the Dirac point, which is consistent with the experimental results.

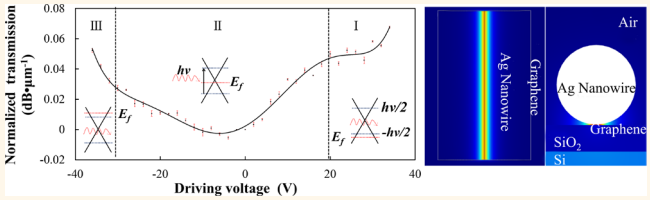

KEYWORDS: graphene · surface plasmon polariton · modulator · nanowire

A surface plasmon polariton (SPP) is an electromagnetic excitation existing and propagating at the interface between a dielectric and a metal. SPPs can be both generated by an irradiating electromagnetic wave with high-energy resolution[1−8] and high-energy electrons with extremely high spatial resolution.[9−11] Due to the ability to produce highly enhanced optical fields below the diffraction limit,[1,2] SPP has wide scientific and technological applications such as SPP lasers,[3,4] optical antennas,[5,6] optical sensors,[7] and subwavelength waveguides.[8] It is desired to have the ability to dynamically manipulate SPPs for their practical applications in modern information and communication technologies, preferably by applying an electrical bias. However, even noble metals, which are widely regarded as the best candidate for plasmonic materials, are hardly tunable simply through electrical operation partially because of the difficulties in changing the carrier density.[12,13] On the other hand, graphene, a two-dimensional sheet of carbon atoms, has shown large potential in achieving electrical control of light, due to its fast carrier velocity and the low carrier scattering rate at room temperature.[13−15] In the past few years, graphene-based infrared and terahertz modulators have been reported by controlling the electronic structure of graphene.[16−22] Most recently, electrical-controlled plasmonic scattering resonance has been demonstrated using the hybrid graphene/metal nanostructure.[23−25] Active tunability of plasmonics transmission has also been achieved by coupling plasmons to optically active materials.[26,27] To our best knowledge, there are few reports on electrical tuning of visible SPP transmission using field effect transistor (FET) structure, because of the extreme challenge due to weak free electron responses, huge transmission losses in this spectral range, and the limited carrier concentration achieved

* Address correspondence to qingyang@zju.edu.cn; zhong.wang@mse.gatech.edu.

Received for review December 3, 2013 and accepted January 31, 2014.

Published online January 31, 2014
10.1021/nn406221s

before the breakdown of the insulator layer in the FET structure.

Very recently, N. K. Emani *et al.*[28] demonstrated control of plasmonic resonances of metal/graphene hybrid structure, which mainly focuses on the plasmonic resonance of graphene in the mid-infrared wavelength and proved that the hybrid structure can enhance light−graphene interactions. Here we report electric tuning of visible-range plasmonic behavior in a grapheme−NW hybrid structure, in which the modulation is achieved through effectively tuning the Fermi level (E_f) of graphene by an externally applied gate voltage. Careful simulation indicates the introduction of Ag NW is important for bringing the response to the visible range: besides the dramatic enhancement of light−graphene interactions, the charge distribution in the graphene is also localized by the Ag NW, which makes the charge density much higher in the vicinity of the NW, approaching 0.921×10^{14} cm^{-2}, enough for tuning light in the visible range. It was thought to be a tough task for a graphene-based FET modulator to tune visible light and could only be achieved by high capacitance ion gel previously because of the contradiction between high carrier density and breakdown of the insulator layer.[29,30] We also compare the electrical-controlling properties of SPPs based on monolayer and bilayer graphene, especially investigating the modulation behavior near the Dirac point of monolayer graphene and the singularity of gap-induced bilayer graphene. The theoretical calculation using the local random phase approximation (RPA) and the tight-binding model shows excellent agreement with experimental results.

RESULTS AND DISCUSSION

Figure 1a shows a schematic diagram of our device structure. A single layer of graphene fabricated using the exfoliation method[31] is first transferred onto the top of a 300-nm-thick SiO_2 layer of a silicon wafer. The graphene is slightly p-doped because of the exposure to oxygen and moisture during the fabrication process of the device.[32] Then the silicon layer and the graphene sheet are connected to a picoammeter (Keithley 6487) for applying bias voltage and electrical measurement. A 500-nm-diameter silver NW is finally placed on the graphene sheet, with its launching port placed outside the graphene sheet to ensure that the coupling efficiency will not be affected by the absorption variation of graphene under modulation (middle inset of Figure 1a). It is possible that the silver NW may have direct carrier transference into graphene considering its work function. In our experiments, the silver NW and graphene are physically contacted. According to the density function theory,[33] the carrier transference between the silver NW and graphene will decrease the Fermi level of the naturally p-doped graphene and keep it p-doped. Thus, the carrier transfer will not change the doping condition and could be neglected in the analysis and simulation. A 659-nm-wavelength laser is used to excite SPPs in silver NW on the graphene sheet through a 100× high numerical aperture (NA = 0.9) objective (Figure S1). The focused light is scattered into guided modes transmitted by the silver NW as SPPs (upper right inset of Figure 1a). The output light is detected by a CCD located on top of the structure. The measured stability of the system shows the time-dependent fluctuation of the laser intensity used in the experiments, which is less than 1% (Figure S2). The monolayer graphene is confirmed by Raman spectroscopy (532-nm-wavelength laser pumping) from the G-peak and 2D-peak features in Figure 1b.[34,35]

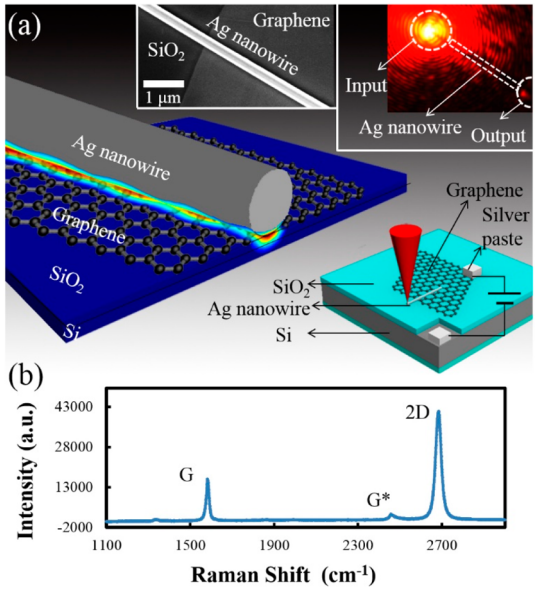

Figure 1. Graphene-based SPP modulator. (a) Three-dimensional (3D) schematic illustration of the device; a graphene sheet is on top of the SiO_2−Si structure. Silver paste is used as electrodes. Insets: middle, scanning electron microscopy (SEM) image of the device; upper right, an optical image of a silver NW on graphene under the excitation of a 659-nm-wavelength laser; lower right, schematic diagram of the whole structure. (b) Raman spectrum of the monolayer graphene.

Figure 2 displays the static electro-optical response of the device characterized under different driven voltages, V_D, when a 659-nm-wavelength light is transmitted through. The experimental data are normalized to the transmissivity value at zero bias voltage. The variation of optical absorption of graphene is determined by the position of the Fermi level through Pauli blocking effects, since interband transition occurs when electrons are excited by the incoming 659-nm-wavelength photons ($h\nu$). The graphene Fermi level can be tuned by applying a driving voltage; thus the total transmission can be modulated electrically. With the current structure design, the modulation depth, which is the logarithm of the ratio of the output light normalized to the NW length under bias voltage to its unbiased

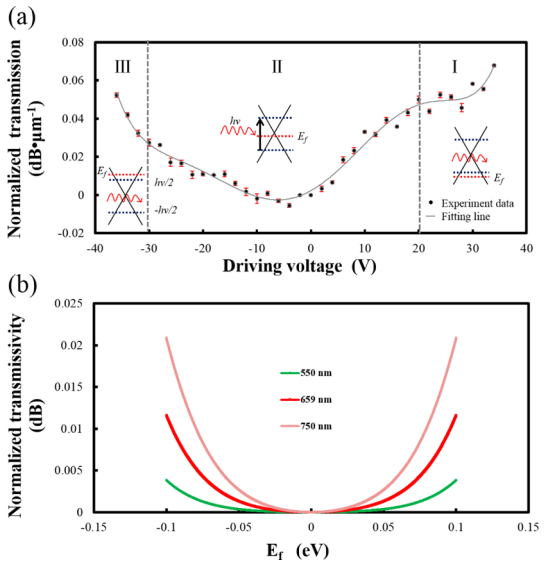

Figure 2. Static electro-optical response of the graphene-based SPP modulator. (a) The main panel shows the modulation depth at different driving voltages, which is normalized to the zero bias transmission (dB/μm). The gray dashed lines represent the boundary of three regions that correspond to the different injection state of the graphene sheet denoted by I, II, and III. Correspondingly, the three insets show the energy band diagram of graphene in the three regions, and the arrow in the inset of region II represents the absorption of an incident photon. All of the data presented were measured 20 times, and the average value is used in the figure for accuracy and reliability. Standard deviation of the measured data is shown in the Supporting Information. (b) Calculated transmissivity of single-layer graphene as a function of Fermi level (E_f) for different wavelengths. The Fermi level can be regarded as a characterization of the driving voltage. In the calculation, the optical conductivity of graphene is defined as a single layer as a whole; thus the transmissivity is a characteristic of the whole monolayer graphene.

level, is as high as 0.07 dB/μm. The total modulation depth of our modulator will reach 3 dB if the interaction distance exceeds 40 μm. Additionally, comparison experiments are carried out on a SiO_2−Si structure without graphene and a SiO_2−Si structure with gold film instead of graphene. No electrical modulation is achieved under the same measurement conditions, which indicates that graphene plays an important role in the modulation process (Figure S3).

Carefully analyzing the static electro-optical response of the device, we find that the response curve can be divided into three parts, regions I, II, and III, respectively. When the device is driven with large positive bias voltage (region I, $V_D > 20$ V, the graphene sheet is injected with an abundance of holes), a sharp increase of the transmission is observed. In this range, the Fermi level is pulled down. Because the occupation density decreases sharply above the Fermi level,[14] when the Fermi level is lower than half of the photon energy, there will be hardly any electron transition due to photon excitation; thus the absorption of the graphene will be decreased and the SPP transmission will be increased. When the device is driven at large negative voltage (region III, $V_D < -30$ V, the graphene sheet is injected with an abundance of electrons), the Fermi level surpasses the Dirac point. When it is higher than half of the photon energy, all electron states interacting with incident photons will be occupied. Owing to the conservation of momentum and limited phonon energy, the newly occupied electrons at high levels of the linear band cannot be excited to even higher levels. Thus, the graphene appears transparent. Theoretically, a sharp increase of transmission should be observed at the Fermi level $E_f = \pm h\nu/2$. However, in reality, defects in the graphene and natural doping will make the transition broaden and shift to higher voltage.[19] When the device is driven under low driving voltages (region II, -30 V $< V_D < 20$ V), the absolute value of the Fermi level is lower than half of the photon energy and intraband transition occurs. According to previous reports,[19] the optical transition in this range is insensitive to the driven voltage V_D. However, in experiments, we find the transmissivity depends on V_D and there is a minimum value near the Dirac point. In order to understand the modulation behavior in range II, we calculate the absorbance A near the Dirac point using the optical conductivity of graphene as a function of Fermi level E_f[36−38] (see Supporting Information, section 5) and plot the curve for normalized transmissivity $10 \log((1 - A)/(1 - A_0)$ for different wavelengths in Figure 2b, where A and A_0 represent the absorption under the driving voltage and $E_f = 0$ eV. In this plot, the Fermi level, expressed in units of eV, can be regarded as a characterization of the driving voltage. It can be seen that the minimum transmissivity occurs at $E_f = 0$ eV. Therefore, there may exist a transmissivity valley near the Dirac point. The calculation also predicts that this transmission decrease will be more obvious in the infrared range.

It is noted that pushing the Fermi level of graphene to the visible range is a very tough task for FET-like structures, and it can be achieved only by liquid ion gel by utilizing its extremely high capacitance density so far.[29,30] The charge accumulated at about 20−30 V using a 300 nm SiO_2 as dielectric layer is not sufficient to shift the Fermi level enough for 659-nm-wavelength light according to the intuition expression.[19] Because the existence of breakdown voltage of the insulator layer, there is a contradiction between the available highest carrier concentration and the avoidance of breakdown. One approach is to use a higher dielectric index liquid ion gel to replace SiO_2. By experimental and simulated investigation, we found the structure used in our experiments is fundamentally different from previous works,[19] and the introduction of Ag NW on graphene will confine the light strongly at the interface and alter the charge distribution in graphene simultaneously, which may provide a new approach to tune the SPP in the visible range. From the simulation shown in Figure 3, we see that the electromagnetic

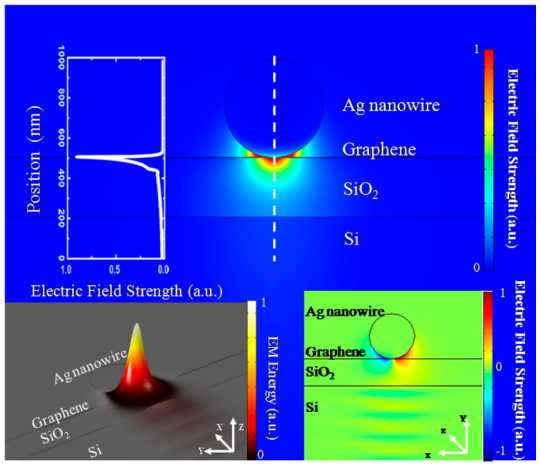

Figure 3. Simulated electric field distribution ($E_x^2 + E_y^2 + E_z^2)^{1/2}$ of the graphene-based SPP modulator using the finite element method. Inset: upper left, electric field intensity at the position denoted by the white dashed line; lower left, the height image of the electromagnetic (EM) energy distribution at the end-face of the SPP modulator; lower right, in-plane electric field distribution $(E_x^2 + E_z^2)^{1/2}$ of the structure, which is very important to the interaction with the graphene sheet. The graphene layer is modeled as a 1 nm thick layer, and the optical conductivity is used as a parameter for simulation. A strongly confined in-plane electric field around the graphene sheet can be seen clearly.

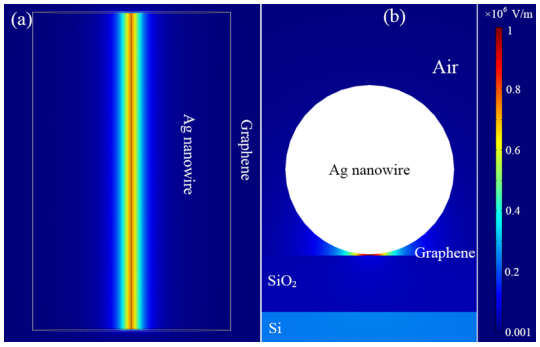

Figure 4. Electric field enhancement at the interface of the Ag NW and the graphene sheet. (a) Top view of simulated electric field distribution in the graphene sheet. White lines denote the Ag NW with 250 nm radius (b) Side view of the simulated electric field distribution of the device.

energy is concentrated at the interface of the Ag NW and the graphene sheet, so that shifting the Femi level of graphene will greatly affect the interaction between graphene and SPPs through Pauli blocking.[39] Besides the light confinement effect, electric field confinement effect under the Ag NW is very important for bringing the optical response of the device to the visible range. The simulation in Figure 4 indicates that the charge density in the vicinity of the NW is much higher than other areas (about 2 orders of magnitude/total effective area) due to different material properties of graphene and silver. We can use the equation $2E_f = 2\hbar v_f(\eta\pi|V + V_0|)^{1/2} = 2\hbar v_f(n\pi)^{1/2}$[19,30] to estimate the Fermi level and the applied voltages. v_f is the Fermi velocity, V is the applied voltage, and V_0 is the voltage

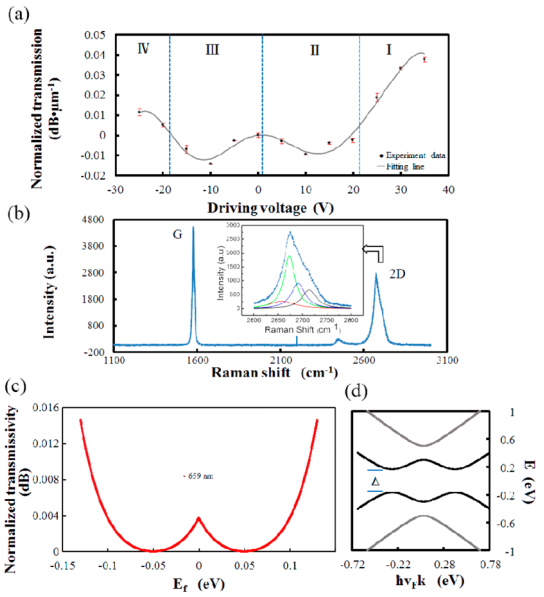

Figure 5. Bilayer graphene-based SPP modulator. (a) Static electro-optical response of the bilayer graphene device at different driving voltages. The data are normalized to the transmissivity with zero bias voltage. All of the data were measured 20 times, and the average value is used in the figure for accuracy and reliability. Standard deviation of the measured data is shown in Figure S5. (b) Raman spectrum of the bilayer graphene. The inset is the 4 Lorenz curve fitting for the 2D-peak. (c) Calculated transmissivity of bilayer graphene as a function of Fermi level (E_f) for 659-nm-wavelengths light. (d) Band structure of the bilayer graphene in the presence of an induced gap Δ. In this calculation, Δ = 0.4 eV and γ = 0.4 eV.

offset caused by the natural doping, and $n = \eta|V + V_0| = C|V + V_0|/e$ represents carrier concentration, where C is the effective capacitance density. The dual-confinement effect of charge density and electromagnetic energy around the vicinity of the NW will dramatically enhance the light−matter interaction and increase the Fermi level shifting. Through calculation and comparison, we estimated the η could be at least 2.63×10^{16} m^{-2} V^{-1} and n reaches 0.921×10^{14} cm^{-2} after applying more than 25 V voltages, which is enough to shift the Fermi level for visible light (see Supporting Information, section 6).

Additionally, we compare the modulation behavior of bilayer and monolayer graphene. Figure 5a shows the modulation experiments based on a bilayer graphene. We identify the number of graphene layers by Raman spectroscopy (using 532-nm-wavelength laser pumping),[34,35] as displayed in Figure 5b. The bilayer graphene still has absorption tunability, and the trend at large negative (region IV) and positive voltage (region I) is similar to the monolayer's. However, some highly repeatable differences exist at low driving voltage. There are two minimum values rather than one minimum value near E_f = 0 eV (regions II and III). The two transmissivity valleys may be attributed to the band gap induced by the driving voltage or impurities in the bilayer graphene.[40] The bilayer graphene has a

shoulder-like band structure and two singularities near the zero momentum (Figure 5d). This singularity has similar properties to the Dirac point, which plays an important role in the modulation process.[40] Calculation results in Figure 5c predict a similar transmissivity behavior near the two singularities (see Supporting Information, section 5).

CONCLUSIONS

In summary, we achieved visible-range SPP modulation through the strong light field and electric field dual enhancement at the interface of a Ag NW and a graphene sheet. The device we fabricated can operate as a 3 dB SPP modulator with a 40-μm-length silver NW. Moreover, the investigation of the modulation behavior provides further understanding of the properties of graphene in the vicinity of the Dirac point and singularity, which may suggest the possibility to realize electrically controlled electron–phonon coupling in graphene.[41] As the SPP mode area can be further squeezed, our device may provide a way of fabricating ultracompact nanophotonic devices and may find its applications in integrated optical circuits, nanoscaled laser sources, optical communications, *etc*. Besides, our device has the potential for dynamic operation and the bandwidth could approach gigahertz when the capacitance of the device is smaller than 0.1 pF.

METHODS

Fabrication Methods. In our experiment, both the monolayer and bilayer graphene are fabricated using the exfoliation method. The substrate for placing the graphene sheet is a silicon wafer covered with 300 nm SiO_2. The number of graphene layers is identified by the Raman spectrum. The silver NW is fabricated by the hydrothermal method. It is transferred and placed on the graphene sheet by precise 3D translation manipulation under an optical microscope. The whole structure is observed by SEM after optical characterization, as shown in the inset of Figure 1.

Measurement System. Our experiment is carried out under an optical microscope. The output light transmitted by the silver NW is collected by the objective and detected by CCD on top of the microscope. We measure the relative intensity of the output light through analyzing the images with the same exposure time for each subexperiment. The measurement system is depicted in Figure S1.

Conflict of Interest: The authors declare no competing financial interest.

Acknowledgment. This work is supported by National Key Basic Research Program of China (No. 2013CB328703), National Natural Science Foundation of China (Nos. 61177062 and 51372220), the Fundamental Research Funds for the Central Universities, the Program for Zhejiang Leading Team of S&T Innovation and the Fundamental Research Funds for the Central Universities, MANA, International Center for Materials Nanoarchitectonics, National Institute for Materials Science, Japan, and a joint project with Sungkyunkwan University, Korea. The authors thank Prof. Xiang Zhang and Dr. Yu Ye at Berkeley and Prof. Shiyou Yang, Junhao He, Pan Wang, and Weisong Yang at ZJU for helpful discussions.

Supporting Information Available: Experimental information, simulation details, and supporting figures and tables. This material is available free of charge *via* the Internet at http://pubs.acs.org.

REFERENCES AND NOTES

1. Schuller, J. A.; Barnard, E. S.; Cai, W.; Jun, Y. C.; White, J. S.; Brongersma, M. L. Plasmonics for Extreme Light Concentration and Manipulation. *Nat. Mater.* **2010**, *9*, 193–204.
2. Barnes, W. L.; Dereux, A.; Ebbesen, T. W. Surface Plasmon Subwavelength Optics. *Nature* **2003**, *424*, 824–830.
3. Sorger, V. J.; Zhang, X. Spotlight on Plasmon Lasers. *Science* **2011**, *333*, 709–710.
4. Kitur, J. K.; Podolskiy, V. A.; Noginov, M. A. Stimulated Emission of Surface Plasmon Polaritons in a Microcylinder Cavity. *Phys. Rev. Lett.* **2011**, *106*, 183903.
5. Knight, M. W.; Sobhani, H.; Nordlander, P.; Halas, N. J. Photodetection with Active Optical Antennas. *Science* **2011**, *332*, 702–704.
6. Alù, A.; Engheta, N. Input Impedance, Nanocircuit Loading, and Radiation Tuning of Optical Nanoantennas. *Phys. Rev. Lett.* **2008**, *101*, 043901.
7. Sannomiya, T.; Dermutz, H.; Hafner, C.; Vörös, J.; Dahlin, A. B. Electrochemistry on a Localized Surface Plasmon Resonance Sensor. *Nano Lett.* **2010**, *26*, 7619–7626.
8. Zhang, S.; Xu, H. Optimizing Substrate-Mediated Plasmon Coupling toward High-Performance Plasmonic Nanowire Waveguides. *Nano Lett.* **2012**, *6*, 8128–8135.
9. Ritchie, R. H. Plasma Losses by Fast Electrons in Thin Films. *Phys. Rev.* **1957**, *106*, 874–881.
10. Wang, Z. L. Valence Electron Excitations and Plasmon Oscillations in Thin Films, Surfaces, Interfaces and Small Particles. *Micron* **1996**, *27*, 265–299.
11. Scholl, J. A.; Koh, A. L.; Dionne, J. A. Quantum Plasmon Resonances of Individual Metallic Nanoparticles. *Nature* **2012**, *483*, 421–427.
12. West, P. R.; Ishii, S.; Naik, G. V.; Emani, N. K.; Shalaev, W. M.; Boltasseva, A. Searching for Better Plasmonic Materials. *Laser Photonics Rev.* **2010**, *4*, 795–808.
13. Koppens, F. H. L.; Chang, D. E.; García de Abajo, F. J. Graphene Plasmonics: A Platform for Strong Light–Matter Interactions. *Nano Lett.* **2011**, *11*, 3370–3377.
14. Neto, A. H. C.; Guinea, F.; Peres, N. M. R.; Novoselov, K. S.; Geim, A. K. The Electronic Properties of Graphene. *Rev. Mod. Phys.* **2009**, *81*, 109–162.
15. Geim, A. K. Graphene: Status and Prospects. *Science* **2009**, *324*, 1530–1534.
16. Fistul, M. V.; Efetov, K. B. Electromagnetic-Field-Induced Suppression of Transport through n-p Junctions in Graphene. *Phys. Rev. Lett.* **2007**, *98*, 256803.
17. Ohta, T.; Bostwick, A.; Seyller, T.; Horn, K.; Rotenberg, E. Controlling the Electronic Structure of Bilayer Graphene. *Science* **2006**, *313*, 951–954.
18. Wang, F.; Zhang, Y.; Tian, C.; Girit, C.; Zettl, A.; Crommie, M.; Shen, Y. R. Gate-Variable Optical Transitions in Graphene. *Science* **2008**, *320*, 206–209.
19. Liu, M.; Yin, X.; Avila, E. U.; Geng, B.; Zentgraf, T.; Ju, L.; Wang, F.; Zhang, X. A Graphene-Based Broadband Optical Modulator. *Nature* **2011**, *474*, 64–67.
20. Rodriguez, B. S.; Yan, R.; Kelly, M. M.; Fang, T.; Tahy, K.; Hwang, W. S.; Jena, D.; Liu, L.; Xing, H. G. Broadband Graphene Terahertz Modulators Enabled by Intraband Transitions. *Nat. Commun.* **2012**, *3*, 780.
21. Chen, J.; Badioli, M.; González, P. A.; Thongrattanasiri, S.; Huth, F.; Osmond, J.; Spasenović, M.; Centeno, A.; Pesquera, A.; Godignon, P.; *et al.* Optical Nano-Imaging of Gate-Tunable Graphene Plasmons. *Nature* **2012**, *487*, 77–81.
22. Fei, Z.; Rodin, A. S.; Andreev, G. O.; Bao, W.; McLeod, A. S.; Wagner, M.; Zhang, L. M.; Zhao, Z.; Thiemens, M.; Dominguez, G.; *et al.* Gate-Tuning of Graphene Plasmons Revealed by Infrared Nano-Imaging. *Nature* **2012**, *487*, 82–85.

23. Kim, J.; Son, H.; Cho, D. J.; Geng, B.; Regan, W.; Shi, S.; Kim, K.; Zettl, A.; Shen, Y. R.; Wang, F. Electrical Control of Optical Plasmon Resonance with Graphene. *Nano Lett.* **2012**, *12*, 5598–5602.
24. Yao, Y.; Kats, M. A.; Genevet, P.; Yu, N.; Song, Y.; Kong, J.; Capasso, F. Broad Electrical Tuning of Graphene-Loaded Plasmonic Antennas. *Nano Lett.* **2013**, *13*, 1257–1264.
25. Xiao, Y.; Francescato, Y.; Giannini, V.; Rahmani, M.; Roschuk, T. R.; Gilbertson, A. M.; Sonnefraud, Y.; Mattevi, C.; Hong, C.; Cohen, L. F.; *et al*. Probing the Dielectric Response of Graphene *via* Dual-Band Plasmonic Nanoresonators. *Phys. Chem. Chem. Phys.* **2013**, *15*, 5395–5399.
26. Temnov, V. V.; Armelles, G.; Woggon, U.; Guzatov, D.; Cebollada, A.; Garcia-Martin, A.; Garcia-Martin, J.-M.; Thomay, T.; Leitenstorfer, A.; Bratschitsch, R. Active Magneto-Plasmonics in Hybrid Metal–Ferromagnet Structures. *Nat. Photonics* **2010**, *4*, 107–111.
27. Dicken, M. J.; Sweatlock, L. A.; Pacifici, D.; Lezec, H. J.; Bhattacharya, K.; Atwater, H. A. Electrooptic Modulation in Thin Film Barium Titanate Plasmonic Interferometers. *Nano Lett.* **2008**, *8*, 4048–4052.
28. Emani, N. K.; Chung, T.-F.; Ni, X.; Kildishev, A. V.; Chen, Y. P.; Boltasseva, A. Electrically Tunable Damping of Plasmonic Resonances with Graphene. *Nano Lett.* **2012**, *12*, 5202–5206.
29. Kim, B. J.; Jang, H.; Lee, S. K.; Hong, B. H.; Ahn, J. H.; Cho, J. H. High-Performance Flexible Graphene Field Effect Transistors with Ion Gel Gate Dielectrics. *Nano Lett.* **2010**, *10*, 3464–3466.
30. Fang, Z.; Thongrattanasiri, S.; Schlather, A.; Liu, Z.; Ma, L.; Wang, Y.; Ajayan, P. M.; Nordlander, P.; Halas, N. J.; de Abajo, F. J. G. Gated Tunability and Hybridization of Localized Plasmons in Nanostructured Graphene. *ACS Nano* **2013**, *7*, 2388–2395.
31. Novoselov, K. S.; Geim, A. K.; Morozov, S. V.; Jiang, D.; Zhang, Y.; Dubonos, S. V.; Grigorieva, I. V.; Firsov, A. A. Electric Field Effect in Atomically Thin Carbon Films. *Science* **2004**, *306*, 666–669.
32. Ryu, S.; Liu, L.; Berciaud, S.; Yu, Y. J.; Liu, H.; Kim, P.; Flynn, G. W.; Brus, L. E. Atmospheric Oxygen Binding and Hole Doping in Deformed Graphene on a SiO_2 Substrate. *Nano Lett.* **2010**, *10*, 4944–4951.
33. Giovannetti, G.; Khomyakov, P. A.; Brocks, G.; Karpan, V. M.; van den Brink, J.; Kelly, P. J. Doping Graphene with Metal Contacts. *Phys. Rev. Lett.* **2008**, *101*, 026803.
34. Ferrari, A. C.; Meyer, J. C.; Scardaci, V.; Casiraghi, C.; Lazzeri, M.; Mauri, F.; Piscanec, S.; Jiang, D.; Novoselov, K. S.; Roth, S.; *et al*. Raman Spectrum of Graphene and Graphene Layers. *Phys. Rev. Lett.* **2006**, *97*, 187401.
35. Malard, L. M.; Pimenta, M. A.; Dresselhaus, G.; Dresselhaus, M. S. Raman Spectroscopy in Graphene. *Phys. Rep.* **2009**, *473*, 51–87.
36. Stauber, T.; Peres, N. M. R.; Geim, A. K. Optical Conductivity of Graphene in the Visible Region of the Spectrum. *Phys. Rev. B* **2008**, *78*, 085432.
37. Mak, K. F.; Sfeir, M. Y.; Wu, Y.; Lui, C. H.; Misewich, J. A.; Heinz, T. F. Measurement of the Optical Conductivity of Graphene. *Phys. Rev. Lett.* **2008**, *101*, 196405.
38. Nair, R. R.; Blake, P.; Grigorenko, A. N.; Novoselov, K. S.; Booth, T. J.; Stauber, T.; Peres, N. M. R.; Geim, A. K. Fine Structure Constant Defines Visual Transparency of Graphene. *Science* **2008**, *320*, 1308.
39. Mak, K. F.; Ju, L.; Wang, F.; Heinz, T. F. Optical Spectroscopy of Graphene: From the Far Infrared to the Ultraviolet. *Solid State Commun.* **2012**, *152*, 1341–1349.
40. Zhang, Y.; Tang, T. T.; Girit, C.; Hao, Z.; Martin, M. C.; Zettl, A.; Crommie, M. F.; Shen, Y. R.; Wang, F. Direct Observation of a Widely Tunable Bandgap in Bilayer Graphene. *Nature* **2009**, *459*, 820–823.
41. McChesney, J. L.; Bostwick, A.; Ohta, T.; Seyller, T.; Horn, K.; González, J.; Rotenberg, E. Extended Van Hove Singularity and Superconducting Instability in Doped Graphene. *Phys. Rev. Lett.* **2010**, *104*, 136803.